

IMECE2015-52270

**MULTILEVEL METAL FLOW-FILL ANALYSIS FOR A CENTRIFUGAL CASTING BASED INDIRECT
ADDITIVE MANUFACTURING OF LATTICE STRUCTURES**

Jiwon Mun¹

Graduate Research Assistant
JiwonMun@my.unt.edu

Matthew Busse¹

Undergraduate Research Assistant
MatthewBusse@my.unt.edu

Jaehyung Ju¹

Assistant Professor
jaehyung.ju@unt.edu

James Thurman²

Associate Professor
james.thurman@unt.edu

¹ Department of Mechanical and Energy Engineering, 1155 Union Circle #311098

² College of Visual Arts and Design, 1155 Union Circle #305100
University of North Texas, Denton, Texas 76203-5017

ABSTRACT

The centrifugal casting is a classical manufacturing method and it has been widely studied. However, when it comes to manufacture thin walled lattice materials with complex three-dimensional meso-structures, a multiscale flow-fill analysis may be needed for macro-filling at the sprue system and micro-filling at lattice structures. On the micro-filing analysis for a thin walled lattice structure, the surface tension of molten metal appears to be an important factor. On the other hand, flow inertia may affect the flow-filling process more than the surface tension of molten metal does. Our hypothesis is that there exist a range of ratios of cell wall thickness to length that are primarily affected by surface tension or density. From comparison with two different molten metals – aluminum and copper alloys, we can estimate the characteristic of flow, which will be of benefit when designing lattice structures and selecting materials for the manufacturing process. The objective of this study is to test the hypothesis by constructing an analytical model on flow filling of molten metals (aluminum alloy and copper alloy) associated with manufacturing lattice structures. The Navier-Stokes equation with surface tension is considered for modeling of the flow of molten metal along the micro-channel of lattice structures and is numerically implemented with MATLAB. Temperature dependent properties of the liquid metals; e.g., density, viscosity, and conductivity, are considered for building the

analytical model. Numerical simulations with a commercial code, ANSYS are conducted using a user defined function. Experimental validation is followed to manufacture a cubic truss lattice structure with a varying wall thickness; 0.5-1mm. Two molten metals - aluminum alloy and copper alloy are used for filling the mold at the centrifugal casting system. The mold is prepared by removing sacrificial lattice patterns made by a polyjet 3D printer. The preliminary result shows that the final lattice structures with an aluminum alloy through the 3D printing of sacrificial pattern followed by centrifugal casting have relatively good flow filling property at thin wall thickness (~0.5mm) due to low surface tension of aluminum alloy. On the other hand, the high surface tension of a copper alloy prevents flow-fill to micro-channel mold cavity, resulting in early solidification. The indirect additive manufacturing based casting shows an excellent surface quality, which can be used for manufacturing cellular structures. A coupled flow and heat transfer of molten metal successfully simulate flow-fill and solidification and is compared with the experiment. Faster filling-time and faster solidification for the temperature-dependent material properties were shown.

Key Words: Additive Manufacturing, Centrifugal Casting, Cellular/lattice Structures, surface tension, micro-scale

1 INTRODUCTION

3D cellular metal structures are increasingly receiving attention for their having combinations of mechanical, thermal, and acoustic properties that provide potential opportunities for diverse multifunctional structural implementation. These include ultra-light structures with high specific strength [1] and high specific strain [2], excellent impact absorption [3], acoustic insulation [4], heat dissipation media and compact heat exchangers [5].

The emerging 3D printing technologies [6] may accelerate the realization of the structural applications of cellular metals. Direct-metal additive manufacturing (AM) processes which use a laser or electron beam over a metal powder -bed are capable of manufacturing fully complex 3D cellular metallic structures. Selective Laser Melting [7], Electron Beam Melting [8], and Direct-metal Laser Sintering [9] are the available direct AM processes to fabricate metallic cellular structures. However, in spite of their capability to fabricate parts with cellular geometries, there are still several constraints in the process, which limits their *scalability* to structural applications. For example, selection of materials is limited: e.g., aluminum alloys are challenging to process due to their high thermal conductivity and high optical reflectivity [10]. Fabricated parts suffer from thermal residual stresses [11]. The 1-D energy based patterning mechanism induces *poor surface finish* mainly by ‘balling’ phenomenon that occurs during laser or electron melting [12]. The ‘balling’ phenomenon limits the direct metal AM process resolution because it causes the formation of discontinuous track, which is responsible for a non-uniform deposition of material on the previous layers, thus inducing *a possible porosity and delamination between layers* that is detrimental to the functional performance of parts such as fatigue [12]. D-AM process also induce anisotropic properties of parts caused by the combined effects of the deposition layer thickness, powder size, power and scanning speed of laser or electron beam [8]. In addition, cost for both machine and manufacturing are extremely high for D-AM processes.

Combining AM with metal casting may be an alternative way to manufacture cellular metals. One may call this “indirect-additive manufacturing (I-AM)”. Some efforts have been made to manufacture lattice metals using I-AM. A tetrahedral Be-Cu alloy lattice structure, with a cell size of 10mm, was fabricated by investment casting of an ABS sacrificial cellular pattern printed by a Fused Deposition modeling (FDM) method [13]. A sand powder based AM was explored to build a lattice metal by combining AM with sand casting [14]. In those studies, the flow fillings of molten metals have not been quantitatively explored yet. In our previous study, we quantitatively investigated flow filling of a molten aluminum alloy at an I-AM; e.g., an investment casting combined with FDM to fabricate a cellular aluminum alloy [15]. The gravity based casting appears to remain a technical challenge to overcome – misrun and porosity caused by sudden solidification of molten metals when it meets network structure with sharp corners of cellular structural molds [14-

16]. Relatively large surface area of cellular structural molds also appears to contribute to sudden cooling, resulting in premature solidification [14-16].

In particular, the liquid metal filling process in the micro-scale capillary channel shows relatively different behavior, compared to typical flow filling process in the channel. That is, the scale and the surface tension effects are should be considered [17-20]. In this study, we explore an alternative I-AM that may overcome the misrun during manufacturing of lattice cellular metals – centrifugal casting of a 3D lattice sacrificial pattern made of a cartable polymer. For the mathematical model, in order to calculate velocity profile, modified N-S equation with surface tension effect in the micro-scale channel for copper and aluminum alloy is compared with the typical N-S equation. For the validation, flow filling simulation is conducted using ANSYS, Fluent. For the experiment, in order to investigate the surface tension effect, the lattice structure having 0.5mm wall diameter with copper and aluminum was cast using centrifugal casting.

2 PREPARATION OF SACRIFICIAL PATTERN WITH AM OF POLYMERS

In this section, we present a method to produce a 3D expendable lattice pattern fabricated by a 3D printer. A polyjet type professional 3D printer (ProJet™ HD 3500 Plus, 3D Systems) was used to produce a cellular pattern. The base material used in the printing is VisiJet® Procast, a castable plastic. The supporting material used for 3D printing is VisiJet® S300, a wax material for hands-free melt away supports.

Mechanical Properties: A 3D printed dumbbell-shaped sample is prepared according to ASTM D638 with an extra high resolution printing mode (16 μm resolution and 750x750x1600 DPI in the x , y , and z directions). A uniaxial test using a universal testing machine (AGS-X Series, Shimadzu) with a load cell of 5kN and a strain rate of 0.001/s shows a modulus of 549MPa and a yield strength of 8.7MPa (Figure 1), which is about 2-20 times higher than waxes in modulus and strength. It should be noted that waxes are generally used as materials for building expendable patterns in investment casting. The relatively high modulus of the base material of the 3D printer is preferred to the conventional wax materials for fabricating 3D expendable cellular patterns with thin walls because the patterns need to bear loads by slurry coating for mold fabrication. The physical properties of VisiJet® Procast are shown in Table 1.

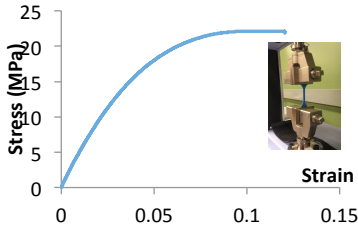


Figure 1. Stress-strain curve of VisiJet® Procast under a uniaxial load at a strain rate of 0.001

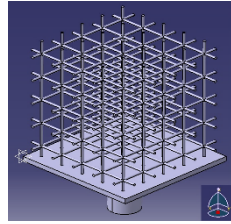


Figure 2. Multifunctional cellular structural pattern with sprue system

CAD drawing and 3D printing: A complex 3D network cellular structure with multifunctional properties; e.g., mechanical and thermal, is pursued to cast with an expendable pattern fabricated by additive manufacturing. A computer aided design (CAD) model for the expendable pattern of a 3D cellular solid with 0.5mm diameter is generated with commercial software, CATIA, as shown in Figure 2. A cellular structural pattern manufactured by a polyjet type 3D printer (ProJet™ HD 3500 Plus) with VisiJet® Procast is printed. The physical properties of VisiJet® Procast are shown in Table 1.

Table 1 Properties of VisiJet® Procast [21]

Density, ρ	Modulus, E	Yield Strength, σ_y	Glass transition temperature, T_g	Melting temperature, T_m	Thermal expansion coefficient, α
1020 kg/m ³	549MPa	8.7MPa	97.59°C	337.11°C	70×10 ⁻⁶ /°C

In terms of its high modulus and low thermal expansion coefficient, VisiJet® Procast has the potential to be used as a base material for fabricating expendable cellular structural patterns over conventional wax materials. Especially, the high modulus is good for building cellular structural patterns with thin cell walls and the low thermal expansion coefficient is favorable for lowering thermal stress during the burning out process of the expendable pattern.

3 PREPARATION OF A GYPSUM PLASTER MOLD SYSTEM

A mold for a sacrificial lattice pattern is prepared with a sprue system. Gypsum ($\text{CaSO}_4 \cdot \frac{1}{2}\text{H}_2\text{O}$) (Satin Cast 20™, FindingKing Kerr) is used for the cubic lattice plaster mold, where the procedure of the mold is shown in Figure 3. A mixture of 100g investment powder (Satin Cast 20™) with 40ml water is prepared, being placed in a vacuum chamber for 2.5 minutes to remove air bubbles inside the mixture. The mixture is poured into the flask covering the sacrificial lattice pattern. The flask is dried in the vacuum chamber for two hours for additional removing of air bubbles. The flask is placed in a furnace to burn out the sacrificial lattice pattern with the following thermal conditions: 149°C for 2 hours, 371°C for 2 hours, 482°C for 2 hours, 732°C for 4 hours and 482°C for 2 hours. A gypsum plaster mold cavity is left after

burning out the sacrificial lattice pattern. Thermo-mechanical properties of the gypsum plaster are shown in Table 2.

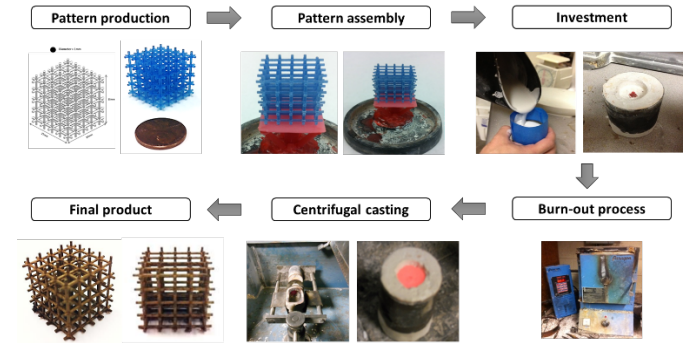


Figure 3. Procedure to manufacture a lattice metal structure using additive manufacturing and centrifugal casting

Table 2 Material properties of gypsum plaster

Property	Value [unit]
Density at 20°C [22]	1,019 [kg/m ³]
Thermal conductivity [22]	0.47 [W/(m * K)]
Specific heat [22]	1570.167 [J/kg * K]
Roughness [23]	2.72×10 ⁻⁶ [m]
Thermal expansion coefficient [22]	7.22 ×10 ⁻⁶ [°C]
Preheated temperature	482 °C

4. CENTRIFUGAL CASTING

4.1 Experimental

Once a cellular structural plaster mold is prepared, a molten metal (copper and aluminum alloys) is prepared for casting. The chemical composition and properties of a molten copper alloy (Jewelry Bronze) and aluminum alloy are shown through Tables 3 to 5, respectively [16].

Table 3 Chemical composition of the copper alloy [16]

Material	Unit					
copper alloy	Chemical Composition (%max, unless shown as range or mean)					
	Cu	Si	Zn	Mg	Pb	
	Min./Max.	91.9	4.0	4.0	0.25 Max	0.25 Max

Table 4 Chemical composition of the aluminum alloy [16]

Material	Unit		
Aluminum alloy	Chemical Composition (%max, unless shown as range or mean)		
	Al	Cr	
	Min./Max.	>99	<0.05

Table 5 Thermo-physical properties of the Cu and Al alloy [16]

Property	Unit	
	Cu alloy	Al alloy
Liquidus temperature	1035 [°C]	660[°C]
Solidus temperature	1005 [°C]	660[°C]
Density	7,200 [kg/m ³] @1200°C	2,340[kg/m ³] @850°C
Specific heat	380 [J/kg * K]	1090 [J/kg * K]
Thermal conductivity	173.07 [W/(m * K)]	94.28 [W/(m * K)] @850°C
Viscosity	0.0038[Pa * s] @1200°C	0.00087 [Pa * s] @850°C
Surface tension coefficient	1500 [N/mm]	900 [N/mm]

A centrifugal casting machine (Rey Motorized Centrifugal Casting Machine, Rey Industries Inc.) was used for casting the copper and aluminum alloys. Figure 4 shows a schematic of the centrifugal casting machine whose width is 70cm, length is 70cm, and height is 90cm. A 30cm casting arm, ③, is rotated with the main shaft, ①, as the center surrounded with the base, ②. The flask sample is installed into the flask cradle, ⑤, held by the flask cradle holding arms, ⑥. The crucible holder, ⑦, accommodating up to 30oz is held by the crucible holding arms to melt the copper and aluminum alloys.

The radial velocity (v_r) of the molten metal into the mold cavity is calculated during the centrifugal casting by measuring the angular velocity of the casting arm (Figure 4). Figure 5 shows the measured RPM of the casting arm. It shows that the rotational speed is stabilized after two seconds. The average RRM measured after two seconds with a tachometer (Tachometer Counter 461920, EXTECH Instruments), was 425.9 ± 58.6 RPM. The measured RPM is used to calculate v_r , which has a relationship with angular velocity, $v_\theta (= \dot{\theta})$:

$$v_r = \dot{\theta}(r^2 - r_0^2)^{1/2} \quad (1)$$

where r is the distance between the center of main shaft and the center of crucible holder and r_0 is the radius of the casting arm.

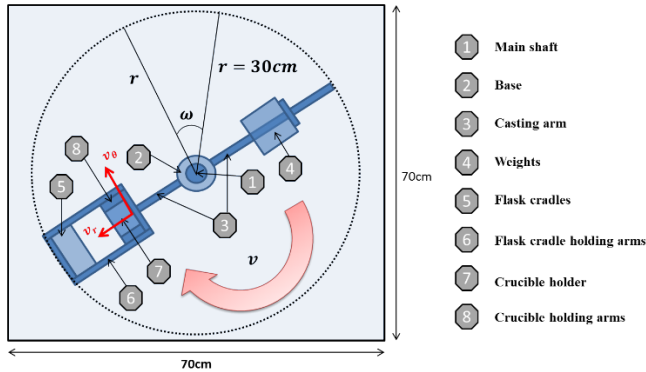


Figure 4. A schematic of the centrifugal casting machine

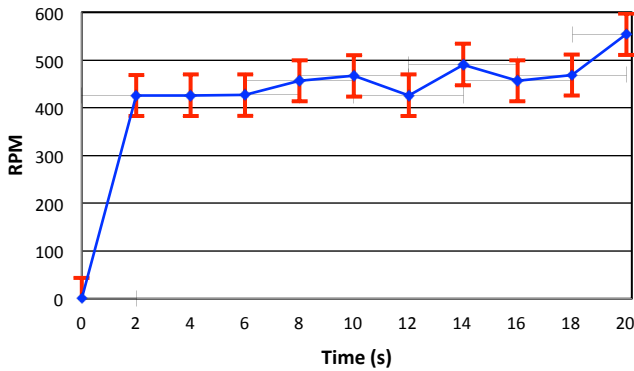


Figure 5. Measured RPM of the centrifugal casting arm

The copper and aluminum alloys are melted by applying heat up to 1,200 °C with an oxygen-acetylene torch, followed by pouring into a crucible holder. Meanwhile, the plaster mold flask, preheated at 482 °C for two hours, is placed in the flask cradle and is balanced by adjusting the location of weight, ④ (Figure 3). Once the rotating procedure is finished, the plaster mold flask is released from the flask cradle, and is cooled down at room temperature for five minutes, followed by quenching in water. Finally, the copper and aluminum alloys lattice structures are obtained by removing the plaster using sand blasting.

4.2 MATHEMATICAL MODELING FOR VELOCITY PROFILE WITH SURFACE TENSION EFFECT IN MICRO-SCALE CHANNEL

4.2.1. MATHEMATICAL MODELING WITH SURFACE TENSION EFFECTS IN MICRO-SCALE CHANNEL

In this study, the lattice part of the metal structure that we are interested in should be considered as micro-scale channel flow due to its scale effect, unlike sprue system. That is, the typical N-S equation can be used for calculating velocity profile in the sprue system. However, for the micro-scale capillary channel flow of the lattice part, The N-S equation should be modified due to its surface tension effect between liquid metal and air phases. Unlike the typical channel flow, the surface tension effect is relatively important because it effects on velocity profile, as shown in Figure 6. The velocity profile is inverted as the liquid metal flows in the micro-scale channel having the angle between liquid metal and air phases, which also make it slow the velocity magnitude of the liquid metal. For the surface traction regime, strong interplay between cohesion and adhesion force is shown. In addition, dynamically evolving contact angle between the interface and channel wall is detected.

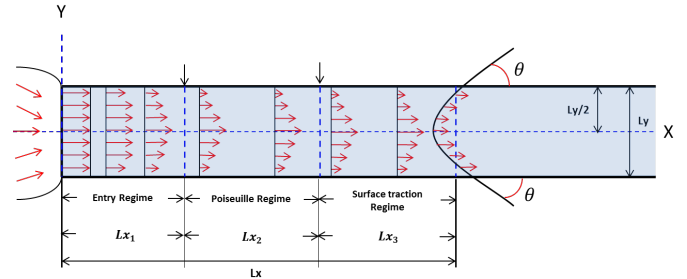


Figure 6. Liquid flow actuation in the micro-scale capillary channel.

The typical N-S equation for continuity and momentum equation are shown as follows:

$$\frac{\partial \rho}{\partial t} + \nabla \cdot (\rho \mathbf{U}) = 0 \quad (2)$$

$$\rho \left(\frac{\partial \mathbf{v}}{\partial t} + \mathbf{v} \cdot \nabla \mathbf{v} \right) = -\nabla p + \mu \nabla^2 \mathbf{v} + \mathbf{f} \quad (3)$$

Where, ρ is the density, \mathbf{v} is the velocity vector, p is the static pressure, \mathbf{f} is the body force (gravity).

For the simplification of N-S equation with surface tension effect in capillary channel, the momentum eq. (2) can

be modified by assuming unsteady flow, infinite supply of liquid without end effects, fully developed laminar flow, incompressible, Newtonian fluid with constant viscosity, and negligible energy dissipation. The modified N-S momentum equation is shown [25].

$$\rho \left(\frac{\partial u}{\partial t} + v \cdot \nabla v \right) = -\nabla p + \mu \nabla^2 v + f + \sigma k \quad (4)$$

where, σ is the surface tension coefficient, k is the curvature of the interface between liquid and air phase in channel.

The curvature (k) between the liquid and air phase can be represented for two dimensional case as follows

$$k = \frac{1}{R} \quad (5)$$

where, R is the radius of the interface between liquid and air phase.

Therefore, the eq. (4) can be represented as follows:

$$\rho \left(\frac{\partial u}{\partial t} + v \cdot \nabla v \right) = -\nabla p + \mu \nabla^2 v + f + \frac{\sigma}{R} \quad (6)$$

In eq. (6), the interface is assumed as half size of sphere in the channel, so R can be represented the half of height of the channel.

In this study, to the N-S equation with and without surface tension coefficient were coded with Matlab.

4.2.2. THE PROPAGATION OF LIQUID PHASE IN CHANNEL

In this section, the propagation of liquid phase in channel for copper and aluminum alloys is compared between the typical N-S equation and modified N-S equation with surface tension effect in micro-scale capillary channel. Figure 7 shows the velocity profile in x direction. The channel has 0.5mm height and 50mm length. The initial injection velocity for Cu and Al alloy are 0.2 m/s and 0.194 m/s (Table 7). The thermo-physical properties of copper and aluminum alloy are shown in Table 5. The time step size is 0.000001 s.

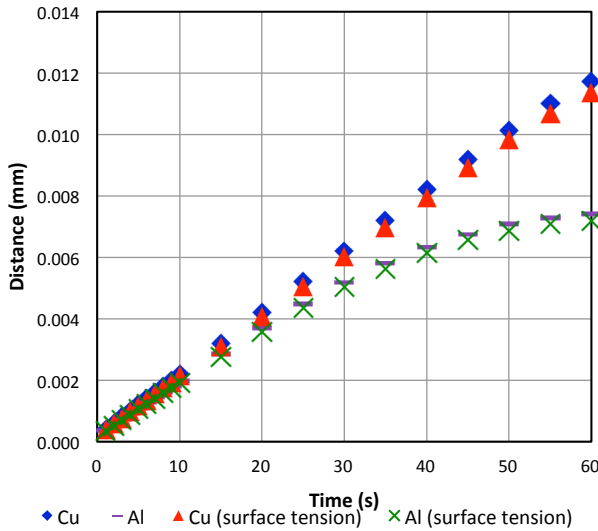


Figure 7. The propagation of the liquid metal as a function of time (d=0.5mm)

The MATLAB code was conducted for 60 minutes for the copper and aluminum with periodic boundary condition. First, the typical N-S equation was performed when there is no surface tension effect. Then, MATLAB code was performed with surface tension effect for copper and aluminum alloys.

Figure 7 shows the distance that the liquid metal flows in the channel as a function of time. There is not much difference on the distance that liquid metal flows in the channel until 10s. However, it is shown that the distance that liquid metal flows with surface tension effect in the channel is shorter than that of without surface tension effect, from around 15s. 3.52E-04mm is shorter for liquid copper and 2.15E-04 mm shorter for liquid aluminum alloy, which shows that the surface tension effect in the channel is more noticeable for the copper alloy rather than liquid aluminum alloy. The distance that liquid aluminum alloy flows in the channel is little bit shorter than that of liquid copper alloy due to the difference on the initial flow velocity. This indicates that the distance that liquid aluminum alloy flows in the channel is further when the initial fluid velocity is the same.

To investigate the surface tension effect according to the size of the diameter of the channel, the MATLAB code was conducted for liquid copper and aluminum alloys with 0.5mm and 1mm diameter.

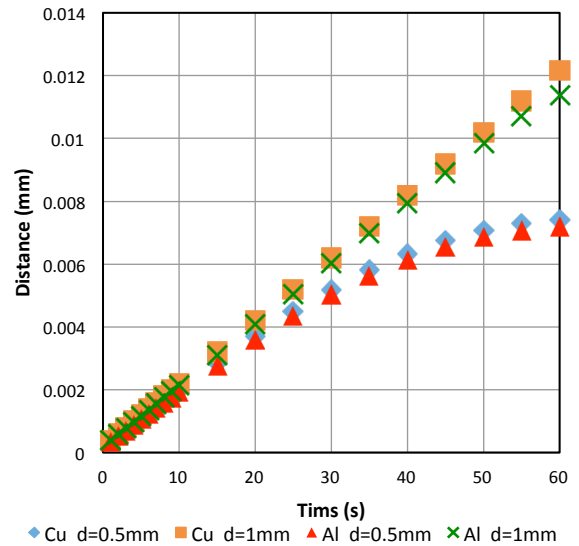


Figure 8. The propagation of the liquid metal as a function of time according to the diameter of channel

Figure 8 shows the propagation of the liquid metal as a function of time according to the diameter of channel. It is shown that the propagated distance of the liquid metal is shorter when the diameter of the channel is 0.5mm for the liquid copper and aluminum alloy. This means that the surface tension effect is more apparent for smaller diameter of the channel, which is due to the fact that the distance that liquid metal flows is inversely proportional to surface tension coefficient and diameter of the channel.

For the mathematical model, the surface tension effect was shown for the simple 2D rectangular channel, which has significantly smaller size. The surface tension effect will be more recognizable in the structure having complex geometry and thin wall thickness, which will be discussed in the next numerical simulation section.

4.3 MODELING AND SIMULATION OF CENTRIFUGAL CASTING

4.3.1 HYDRODYNAMICS OF THE MOLTEN METAL FLOW

We obtain the initial velocity at crucible holder from Equation (1) using the initial radial velocity of molten metal caused by rotation of the casting arm. The obtained inlet velocity at the sprue ((1) in Figure 9) is 8.028 m/s, which will be used to calculate the inlet velocity into the lattice mold ((4) in Figure 9).

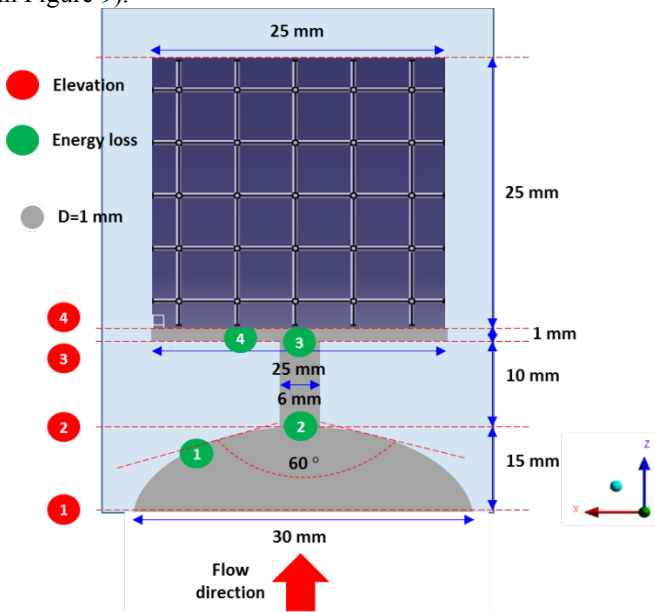


Figure 9. A schematic of a sprue system with a cubic lattice mold to estimate the flow speed of molten metal

In searching the inlet velocity into the lattice mold, the Bernoulli equation with losses is considered to estimate the flow speed of molten metal after being poured at the sprue system ((1)-(4) Figure 9):

$$H_1 + \frac{P_1}{\rho g} + \frac{V_1^2}{2g} = H_2 + \frac{P_2}{\rho g} + \frac{V_2^2}{2g} + \left(f \frac{L}{D} + \sum K\right) \frac{V_2^2}{2g} \quad (13)$$

where, H is the height between points of interest, P is the pressure, ρ is the density of molten metal, g is the gravitational acceleration, V is the velocity of molten metal, f is the frictional coefficient associated with viscosity of molten metal, L is the length of channel, D is the diameter of channel, and K is the minor loss coefficient at the bend or exit. It should be noted that the energy loss by interface friction associated with resistance of the mold walls to the passage of molten metal is not considered.

Table 6 shows the relative roughness, the friction coefficient, f , and the minor loss coefficient, K , at the sections of the sprue system, which can be used for Equation (13) to estimate the flow at each section.

Table 6 Losses used in the lattice structure in Figure 9

Section	Relative roughness (ϵ/D)	Friction Coefficient (Moody chart)	Minor losses coefficient
1-2	9.067×10^{-5}	1.4×10^{-2}	Gradual contraction $\rightarrow k = 0.032$
2-3	4.50×10^{-4}	2.04×10^{-2}	Entry loss (chamfered inlet) $\rightarrow k = 0.25$
3-4	1.08×10^{-4}	1.51×10^{-2}	Entry loss (square-edged inlet)+sudden expansion $\rightarrow k = 0.5 + 0.86 = 1.36$

The velocity at the elevation (4) (Figure 9) is obtained by dividing with the number of holes of the lattice structure (25 holes). The corresponding Reynolds numbers were obtained to determine the flow type at each point. It is found that the flow is laminar through the entire lattice structure. It should be noted that the critical inlet speed of the molten copper and aluminum alloys to overcome solidification inside the mold velocity at the elevation (4) for both Cu and Al alloy cavity can also be traced with Eq. (1) and Table 6. The initial are 0.2 m/s and 0.194 m/s, respectively. The flow regime for lattice part shows laminar flow for both Cu and Al alloy.

Table 7. Reynolds numbers to identify flow type

Section	Velocity Magnitude (m/s)	Reynolds number ($2300 \leq Re\# \leq 4000$)
Cu alloy		
1-2	$V_1 = 8.028$	$456,328.42 \rightarrow$ Turbulent
2-3	$V_2 = 7.858$	$89,333.053 \rightarrow$ Turbulent
3-4	$V_3 = 7.715$	$365,447.368 \rightarrow$ Turbulent
	$V_4 = 5.021/25 = 0.2$	$189.474 \rightarrow$ Laminar
Al alloy		
1-2	$V_1 = 8.028$	$647,776.552 \rightarrow$ Turbulent
2-3	$V_2 = 7.858$	$126,811.862 \rightarrow$ Turbulent
3-4	$V_3 = 7.452$	$501,082.759 \rightarrow$ Turbulent
	$V_4 = 4.85/25 = 0.194$	$260.897 \rightarrow$ Laminar

4.3.2 FLOW SIMULATION THROUGH THE LATTICE STRUCTURAL MOLD

Due to the complexity of flow of molten metal into the lattice structural mold, we use ANSYS/FLUENT, a commercial finite difference code [24]. The inlet velocity at the lattice structural mold (at (4) in Figure 9) is used with the value obtained from the macro-flow estimation in Eq. (13). As determined in the previous section, a fully developed laminar flow is applied to the liquid metal flow into the lattice structural mold in the micro-flow analysis (Table 7).

An unsteady momentum equation coupled with an unsteady heat transfer is applied to the microscopic flow simulation of the molten copper alloy through the cellular structural mold cavity. A Newtonian flow property, isotropy, and incompressibility of the molten copper and aluminum alloy were applied to the flow filing simulation with laminar flow option. The conduction heat transfer is applied in the flow simulation.

Volume of fluid (VOF) method for flow fill

To describe interphase between solid and liquid phases, the VOF method was used. This enables tracking of the transition of the interfaces with arbiter topology and deformation [24].

To define the fractional volume of each phase in the computation domain, the time derivative of $F(\mathbf{x}, t)$ is expressed as:

$$\frac{\partial F}{\partial t} + \mathbf{V} \cdot \nabla F = 0 \quad (14)$$

This function has a range from zero to the unity ($0 < F < 1$). $F = 0$ indicates that a cell contains no fluid, $F = 0.5$ indicates the interphase between liquid and solid phases, and $F = 1$ means that a cell is full of fluid.

4.3.3 FLOW-FILL SIMULATION RESULTS

Due to the complexity of flow of molten metal in the lattice structural mold, we use ANSYS/FLUENT, a commercial finite difference code [24]. The inlet velocity at the lattice structural mold (at 4 in Figure 9) is used with the value obtained from the previous equation with Eq. (13). As determined in the previous section, a fully developed laminar flow is applied to the metal flow into the lattice structural mold (Table 7). An unsteady momentum equation coupled with an unsteady heat transfer is applied to the flow simulation of the copper and aluminum alloys through the lattice structural mold cavity (Figure 10). A Newtonian flow property, isotropy, and incompressibility of molten liquid metal were considered during the simulation. Laminar flow option and conduction heat transfer are applied in the flow simulation as well (Table 7).

Coarse meshes consisting of 1,410,385 elements and 315,111 nodes with a minimum mesh size of $1.5161 \times 10^{-5} m$ are generated. The properties of the cellular plaster mold are shown in Table 2. If the molten metal flows through thin tubes, which is the case of this study with surface tension effect. The surface tension effect might be more sensitive rather than thicker tube. In this paper, we use constant material properties for liquid metals. To save the time for simulation, the lattice structure of interest is reduced into quarter size of the original lattice structure, as shown in Figure 10. The sliced planes along the yz and zx axis are applied as symmetry for boundary conditions. The initial temperature of the molten metal is 1200°C for both of Cu and Al alloy and the initial temperature of the lattice mold is maintained as 482°C.

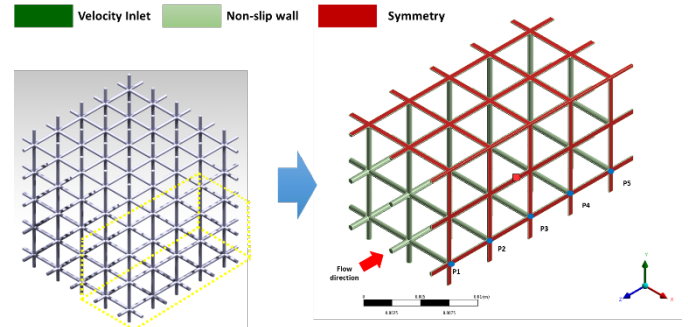


Figure 10. A schematic of flow simulation of a molten metal in the lattice structural mold

Flow-fill of molten liquid metal through the plaster mold is simulated with surface tension effect (Table 5) as a function of time. In order to systematically analyze the volume fraction (the degree of flow-filling), the five points are monitored with the flow-filling time during the simulation time, as shown in Figure 10.

Figure 11 shows the degree of flow-filling at the five points of interest. Filling time at the local points of interest can be obtained from the flow-fill simulation. From Figure 11, it is shown that the molten aluminum alloy is fully filled in the lattice structure around 7s. On the other hand, the molten copper alloy is not filled in the lattice structure having 0.5mm diameter. This can be explained by their thermo physical material properties as shown in Table 5. That is, the reason why the molten aluminum alloy is filled in the lattice structure is might due to the fact that it has less viscosity and surface tension coefficient, compared to the molten copper alloy.

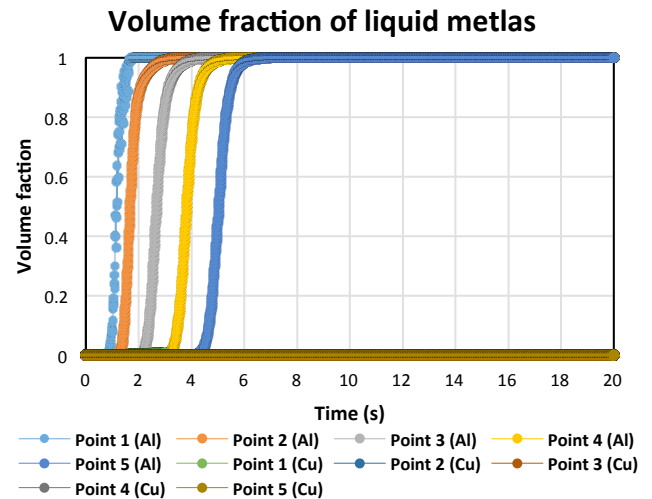


Figure 11. Volume fraction for Cu and Al alloy as a function of time

The molten aluminum has 8 times less viscosity and 1.5 times less surface tension coefficient, which make the molten aluminum fills the lattice tube in the lattice structure, although its initial velocity (0.194 m/s) is less than that (0.2m/s) of the molten copper alloy. In addition, the Reynolds number of the

molten aluminum alloy in the lattice mold shows higher value rather than that of the molten copper alloy. This means that the local velocity in the lattice channel is higher to be filled the lattice mold, as compared to the molten copper alloy.

5 CONCLUDING REMARKS

An indirect additive manufacturing method combining 3D printing technology and centrifugal casting was suggested and was implemented to manufacture a multifunctional 3D cellular copper and aluminum alloy with a quantitative study on flow simulation of molten metal. A 3D cellular structural pattern was built with 3D printing of VisiJet® Procast, followed by molding and centrifugal casting. The mathematical model was suggested with modified N-S equation considering surface tension effect in lattice channel, using commercial MATLAB code. Also, surface tension effect was investigated according to diameter of lattice channel using mathematical model. For the numerical approach, filling simulation of molten metal during the centrifugal casting process were simulated in the cellular structural plaster mold cavity having 0.5mm thickness over a range of running temperature (480°C~1200°C). Constant material properties of molten metal and plaster mold were applied for simulation of flow-fill in ANSYS/FLUENT. The major findings through this study are

- Surface tension effect is more recognizable for the lattice channel having thinner diameter. The distance the liquid metal propagates in the lattice channel showed shorter propagation for the lattice channel having 0.5mm diameter due to the higher surface tension effect.
- The liquid aluminum alloy was relatively fully filled in the lattice structure for flow-filling simulation. However, the lattice structure was not filled with the liquid copper alloy. This is due to the fact that the liquid copper alloy has higher viscosity and surface tension coefficient, which makes diminish the fluid velocity in terms of Reynolds number in the lattice channel.

6 ACKNOWLEDGEMENTS

The study received a support from the Research Seed Grant (RSG) of the Vice President for Research and Economic Development at the University of North Texas (UNT). The authors also thank PACCAR Technology Institute and KCIS, Co. Ltd for partially supporting this study.

REFERENCES

1. Gibson L.J. and Ashby, M. F., 1997, Cellular Solids-Structure and properties, *Cambridge University Press*, Cambridge, UK.
2. Ju, J., Summers, J.D., Ziegert, J., and Fadel, G., 2012, Design of Honeycombs for Modulus and Yield Strain in Shear. *Transactions of the ASME: J. Eng. Mater. & Tech.* **134**(1), pp. 11-22.
3. Tan, H., and Qu, S., 2010, Chap 6: Impact of Cellular Materials. *Cellular and Porous Materials in Structures and Processes*. CISM International Centre for Mechanical Science, Springer.
4. Phani, A. S., Woodhouse, J., and Fleck, N.A., 2006, Wave Propagation in Two-Dimensional Periodic Lattices. *J. Acoustical Society of America*, **119**(4), pp. 1995-2005.
5. Kumar, R. S., and McDowell, D.L., 2004, Rapid Preliminary Design of Rectangular Linear Cellular Alloys for Maximum Heat Transfer. *J. AIAA*, **42**(8), pp. 1652-1661.
6. Kruth, J.P., Leu, M.C., and Nakagawa, T., 1998, Progress in Additive Manufacturing and Rapid Prototyping. *CIRP Annals – Manufacturing Technology*, **47**(2), pp. 525-540.
7. Mullen, L., Stamp, R.C., Brooks, W.K., Jones, E., and Sutcliffe, C.J., 2009, Selective Laser Melting: A Regular Unit Cell Approach for the Manufacture of Porous, Titanium, Bone In-Growth Constructs, Suitable for Orthopedic Applications. *J. of Biomedical Materials Research Part B: Applied Biomaterials*, **89**(B), pp. 325-334.
8. Murr, L.E., et al., 2011, Next-Generation Biomedical Implants using Additive Manufacturing of Complex, Cellular and Functional Mesh Arrays. *Phil. Trans. R. Soc. A.*, **368**, pp. 1999-2032.
9. Murali, K., et al., 2003, Direct Selective Laser Sintering of Iron-Graphite Powder Mixture. *J. of Materials Processing Technology*, **136**, pp. 179-185.
10. Lott, P., et al., 2011, Design of an Optical System for the In-Situ Process Monitoring of Selective Laser Melting (SLM). *J. of Physics Procedia*, **12**, pp. 683-690.
11. Song, B., Dong, S., Liu, Q., Liao, H., and Coddet, C., 2014, Vacuum Heat Treatment of Iron Parts Produced by Selective Laser Melting: Microstructure, Residual Stress, and Tensile Behavior. *J. of Materials and Design*, **54**, pp. 727-733.
12. Yadroitsev, I., and Smurov, I., 2011, Surface Morphology in Selective Laser Melting of Metal Powders. *J. Physics Procedia*, **12**, pp. 264-270
13. Chiras, S., et al., 2002, The Structural Performance of Near-Optimized Truss Core Panels. *J. of Solids and Structures*, **39**, pp. 4093-4115.
14. Meisel, N.A., Williams, C.B., and Druschitz, A., 2014, Lightweight Metal Celluar Structures via in Direct 3D Printing and Casting. In *Proceedings of the 24th Solid Freeform Fabrication Symposium*, Austin, TX.
15. Craig, R.G., Eick, J.D., and Peyton, F.A., 1967, Strength Properties of Waxes at Various Temperatures and Their Practical Application. *J. of Dental Research*, **461**(1), pp. 300-305.
16. Metals handbook Ninth Edition, Volume 2 Properties and Selection: Nonferrous Alloys and Pure Metals., 1979, *American Society for Metals*, Metals Park. Ohio 44073.
17. Ming-xing Ren, Guo-tian Wang, Bang-sheng Li, Zhen-long Wang, and Heng-zhi Fu, 2013, Flow equation and similarity criterion during centrifugal casing in micro-channel, *J. of Trans. Nonferrous Met. Soc. China*, **24**(2014), pp. 1506-1511.

18. G. Hetsroni, A. Mosyak, E. Pligrebnyak, L.P. Yarin, 2005, Fluid flow in micro-channels, *Int. J. of Heat & Mass Transfer*, **48**(2005), pp. 1982-1998.
19. W.R. Jong, T.H. Kuo, S.W. Ho, H.H. Chiu, S.H. Peng, 2006, Flows in rectangular micro channels driven by capillary force and gravity, *Int. J. of Communications in Heat & Mass Transfer*, **34**(2007), pp. 186-196.
20. Lung-Jieh Yang, Tze-Jung Yao, and Yu-Chong Tai, 2003, The marching velocity of the capillary meniscus in a microchannel, *J. of Micromech. Microeng.*, **14**(2004), pp. 220-225.
21. J. Mun, J. Ju, J. Thurman, 2014, Indirect Additive Manufacturing Based Casting of Bronze Cellular Solids, In *Proceedings of the ASME International Mechanical Engineering Congress and Exposition*, IMECE2014-38055, Montreal, Canada.
22. P. Tesarek, J. Drchalova, J. Kolisko, P. Rovnanikova, R. Cerny, 2004, Mechanical, Hygric and Thermal Properties of Flue Gas Desulfurization Gypsum, *J. of Advanced Engineering, Acta Ploytechnica*, **44**(5-6), pp. 83-88.
23. Yi-Chih Chang, Chien-Hung Yu, Wen-Miin Liang, Ming-Gene Tu, San-ue Chen, 2012, Comparison of the surface roughness of gypsum models constructed using various impression materials and gypsum products, *J. of Dental Sciences*, In Press, Corrected Proof, pp. 1-6.
24. Ansys 14.5 FLUENT Theory Guide, 2012, ANSYS Inc.
25. Nils Thurey, Chris Wojtan, Markus Gross, Greg Turk, 2010, A multiscale approach to mesh-based surface tension flows, *ACM transaction on Graphics, Proceedings of ACM SIGGRAPH 2010*, Vol. 29 (4), pp. 1-9.